# High Performance GdTi$_x$O$_y$ Electrolyte-Insulator-Semiconductor pH Sensor and Biosensor

*Jim-Long Her[1], Min-Hsien Wu[2], Yen-Bo Peng[3], Tung-Ming Pan[3,\*], Wen-Hui Weng[4], See-Tong Pang[5], Lifeng Chi[6]*

[1] Division of Natural Science, Center for General Education, Chang Gung University, Taoyuan 333, Taiwan, R. O. C.
[2] Graduate Institute of Biochemical and Biomedical Engineering, Chang Gung University, Taoyuan 333, Taiwan, R. O. C.
[3] Department of Electronics Engineering, Chang Gung University, Taoyuan 333, Taiwan, R. O. C.
[4] Department of Chemical Engineering & Biotechnology, Institute of Biotechnology, National Taipei University of Technology, Taipei 10608, Taiwan, R. O. C.
[5] Division of Urology, Chang Gung Memorial Hospital, Taiyuan 333, Taiwan, R. O. C.
[6] Institute of Physics, Westfälische Wilhelms-Universität Münster, 48149 Münster, Germany
[\*]E-mail: tmpan@mail.cgu.edu.tw

In this paper, we report an electrolyte–insulator–semiconductor (EIS) device incorporating Gd$_2$O$_3$ and GdTi$_x$O$_y$ sensing films deposited on Si substrates through reactive radio frequency sputtering for biomedical engineering applications. We employed X-ray diffraction, X-ray photoelectron spectroscopy, and atomic force microscopy to investigate the structural and morphological features of these films with annealing at various temperatures. Compared with Gd$_2$O$_3$ sensing membrane, the EIS device featuring GdTi$_x$O$_y$ sensing membrane annealed at 900 °C exhibited a higher sensitivity (64.13 mV/pH in the solutions from pH 2 to 12), a smaller hysteresis voltage (1 mV in the pH loop 7→4→7→10→7), and a lower drift rate (0.4 mV/h in the pH 7 buffer solution). This outstanding pH sensitivity may be attributed to the high surface roughness of sensing film. Finally, we successfully demonstrated the use of EIS with glucose oxidase-immobilized alginate film for the detection of glucose in serum. The concentration of serum glucose measured by a GdTi$_x$O$_y$ EIS biosensor is comparable to that determined by commercial assay kit. The GdTi$_x$O$_y$ glucose biosensor can detect glucose with reasonable sensitivity (8.37 mV/mM) in solutions containing glucose at concentrations in the range 0.5–6 mM; this sensitivity is adequate for general clinical examination of blood glucose.

## 1. INTRODUCTION

The ion–selective field–effect transistors (ISFETs) have been used popularly as biochemical and pH sensors since they were first demonstrated by Bergveld in 1970's [1-3]. Electrical potential produced by ions at the oxide–electrolyte interface modulates the current in the ISFET's channel, which is similar to the operating mechanism of the traditional metal–oxide–semiconductor field–effect transistors (MOSFETs). The MOSFET device consists mainly of the metal, oxide, semiconductor substrate, and source/drain; the difference between an ISFET and a MOSFET device is that no metal gate electrode is employed in the former. Electrolyte–insulator–semiconductor (EIS) sensor, the counterpart of ISFET, has several advantages over ISFET including less expensive and easier fabrication. The change in the chemical composition of the analyte will induce variation in the electrical surface charge of the capacitive EIS device, consequently modulating the capacitance of the EIS sensor [3]. Therefore, such an EIS sensor is a promising candidate biosensor for evaluating the sensing characteristics of membranes such as pH sensitivity, hysteresis, and drift [4-5].

Because of the high tunneling current, the conventional $SiO_2$ will be no longer suitable for gate dielectrics when the CMOS transistor is scaled down to nano regime with the effective oxide thickness less than 1nm [6]. The tunneling current directly influences the gate reliability and draws the extra steady state current [7]. To overcome these problems, high dielectric constant (high-κ) materials with a thicker physical thickness will replace $SiO_2$ as gate dielectrics in the future generation CMOS devices [6-7]. Rare-earth (RE) oxide film has emerged as one of the most promising high-κ gate dielectrics to substitute gate oxide $SiO_2$ due to its high dielectric constant, high resistivity, and large bandgap energy [8-10]. The main concerns of RE oxide films include silicate formation, hygroscopicity, and formation of O vacancies [8]. The formation of RE silicate on Si may occur by Si diffusion from the substrate [11]. The tendency to form silicate decreases with decreasing ionic radii due to volume constraints. The hygroscopicity of RE oxides decreases with decreasing ionic radii and scales inversely with RE electronegativity [12]. Among the RE oxides, $Gd_2O_3$ film can be considered for high-κ gate dielectric applications because of its lattice match to Si, good thermal stability with Si, and large conduction and valence band offsets [13-14]. To minimize moisture absorption and silicate formation, the addition of Ti or $TiO_2$ into the RE dielectric films can cause improved physical and electrical properties (a thinner interfacial layer, lower solubility in water, higher capacitance, and lower leakage current) because it reduces the extent of the reaction of the dielectric film with water and Si substrate [15-17]. In this paper, we described the structural and sensing characteristics of $Gd_2O_3$ and $GdTi_xO_y$ sensing films deposited on Si substrates by means of reactive radio frequency (rf) sputtering. We applied X-ray diffraction (XRD) to determine the growth directions and crystallinity of the films, atomic force microscopy (AFM) to monitor the surface morphology of the $Gd_2O_3$ and $GdTi_xO_y$ films, and X-ray photoelectron spectroscopy (XPS) to analyze the chemical structure of the sensing films after annealing at different temperatures. Furthermore, we determined the effect of post-deposition annealing (PDA) treatment on the sensing characteristics (pH sensitivity, hysteresis, and drift) of the $Gd_2O_3$ and $GdTi_xO_y$ films. Finally, we demonstrate that the hybrid configuration of a $GdTi_xO_y$-based EIS with an attached glucose oxidase–immobilizing alginate hydrogel allows for the detection of

glucose. The concentration of serum glucose measured by a $GdTi_xO_y$ EIS biosensor is nearly identical to that determined by commercial assay kit.

## 2. EXPERIMENTAL

### A. *Fabrication of EIS pH sensor*

EIS devices with $Gd_2O_3$ and $GdTi_xO_y$ sensing membranes were fabricated on a 4-in p-type (100) silicon wafer with a resistivity of 5-10 $\Omega$–cm. Before the deposition of sensing film, the wafer was cleaned with a standard Radio Corporation of America (RCA) process and then immersed in a dilute 1% HF solution for 30 s to remove the native oxide layer. A ~40 nm $Gd_2O_3$ film was deposited on the Si substrate by reactive rf sputtering from a gadolinium oxide target in diluted $O_2$ ambient ($Ar/O_2$=5 sccm/2 sccm) at a substrate temperature of 27 °C, whereas a ~40 nm $GdTi_xO_y$ film was deposited by reactive rf cosputtering from both gadolinium and titanium targets in the same diluted $O_2$ condition. All samples were annealed in a rapid thermal annealing under ambient $O_2$ condition at selected reaction temperature (700~900 °C) for 30 s. The structure and composition of the $Gd_2O_3$ and $GdTi_xO_y$ films after PDA at different temperatures were analyzed by using XRD and XPS. In the XRD and XPS analysis, Cu $K_\alpha$ ($\lambda$ =1.542 Å) radiation and monochromatic Al $K_\alpha$ (1486.7 eV) source are used, respectively. The surface roughness of $Gd_2O_3$ and $GdTi_xO_y$ films was measured using AFM in tapping mode operation. Then, an Al film (~400 nm) was deposited onto the rear of the wafer to act as the backside contact by using thermal evaporation method. The micropatterns on $Gd_2O_3$ and $GdTi_xO_y$ membranes were fabricated by spin-coating a layer of photoresist (SU8-2005 from MicroChem Inc. USA) on the $Gd_2O_3$ and $GdTi_xO_y$ films, and by photolithographic processing to define the sensing zone in $Gd_2O_3$ and $GdTi_xO_y$ membranes. The as-fabricated EIS device was attached to printed circuit board (PCB) with Cu electrode by using a silver gel and then was encapsulated by an epoxy resin.

### B. *pH sensing performance of EIS sensor*

Before the pH measurements, EIS device was incubated in reversed osmosis water (R.O.) for 12 h to saturate the ionic properties of the tested sensing membrane. In the pH sensing experiments, the as-fabricated EIS sensor was immersed in various pH buffers (pH 2~12, Merck Inc. USA) together with an Ag/AgCl reference electrode. Capacitance-voltage (C-V) measurements in various pH buffers were performed with Hewlett-Packard (HP) 4284A LCR meter. An ac voltage with the amplitude of 20 mV and the frequency of 100 Hz has been used in all measurements. Moreover, pH sensing experiments were performed in a dark condition to avoid the interference caused by the ambient light and noise.

### C. *Detection of serum glucose using EIS sensor with enzyme layer*

Before the detection of serum glucose, a layer of glucose oxidase-immobilized alginate hydrogel (1 mm) was attached onto the top of $GdTi_xO_y$ sensing film. Briefly, 1X phosphate buffered saline (1X PBS) containing glucose oxidase (from Jack Beans, ~100 U/mg: unless otherwise stated all

chemicals were purchased from Sigma) was thoroughly mixed with an alginate suspension to form a glucose oxidase/alginate suspension with the resulting concentration of 0.1 mg/L. The mixed solution was then loaded onto a clean glass slide and followed by covering with another glass slide with a 1 mm thick spacer in between, allowing the definition of the thickness of alginate thin layer. In the gelatinization process, the sandwich-like structure was incubated in 102 mM $CaCl_2$ solution for 10 min. Finally, the enzyme-containing alginate gel was shaped according to the sensing zone of $GdTi_xO_y$ sensing film and subsequently attached onto the oxide surface. Glucose standard solutions with different concentrations (0.5~6 mM) were made using 1X PBS and the pH level of each analyte was checked to be equal by a pH meter. In the sensing experiments of glucose, EIS sensor with a layer of enzyme membrane was incubated in the analyte for 10 min and then C-V plot was recorded. The device was thoroughly rinsed with R.O. water after each measurement. For the detection of serum glucose, the serum was firstly diluted 2 times by 1X PBS and the resulting analyte was then examined by a $GdTi_xO_y$ EIS biosensor based on the above-mentioned procedures. Furthermore, the concentration of diluted serum glucose was also checked by a commercial glucose assay kit (MeDiPro, Taiwan). Briefly, the serum sample was mixed with the assay reagents for 5 min, and then the absorbance of mixed solution was recorded in the wavelength of 505 nm. The concentration of glucose in serum can be determined by comparing its absorbance with the one from standard sample.

## 3. RESULTS AND DISCUSSION

### 3.1. Structural properties

A detailed investigation of the crystalline structure of the $Gd_2O_3$ and $GdTi_xO_y$ films before and after PDA treatment was understood by XRD measurements as shown in Figs. 1(a) and (b). A strong (622) peak and two weak (440) and (145) peaks are observed for the as-deposited $Gd_2O_3$ sample, which means that the film is a polycrystalline structure. In contrast, for the $GdTi_xO_y$ sample, no peak was found in the 2θ diagram, indicating an amorphous structure. The temperature-induced of the crystalline structure of $Gd_2O_3$ and $GdTi_xO_y$ films can be followed by XRD analysis. The intensity of three (440), (145), and (622) diffraction peaks for $Gd_2O_3$ film increased with increasing the PDA temperature, possibly suggesting that the film is condensed during this annealing temperature to form a stoichiometric $Gd_2O_3$ film. However, the high temperature annealing will easily produce the formation of an amorphous silica and/or a nonstoichiometric silicate layer at the oxide/Si interface [8]. In contrast, one strong $GdTiO_3$ (132) peak and two weak $GdTiO_3$ (211) and (311) peaks were found in the annealed $GdTi_xO_y$ sample, as shown in Fig. 1(b). Besides the peaks mentioned above, the film annealed at 900 °C had a $Gd_2Ti_2O_7$ (222) peak in the 2θ diagrams, indicative of a preferential orientation of the crystallites with the (222) planes of $Gd_2Ti_2O_7$ parallel to the substrate.
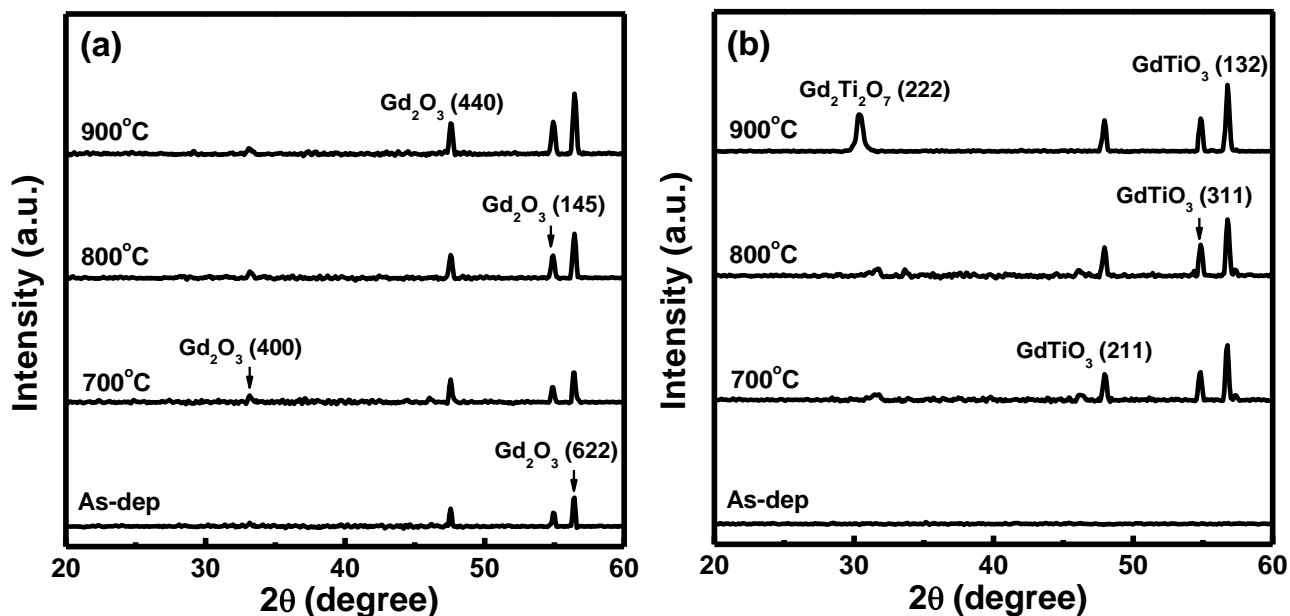
**Figure 1.** XRD patterns of (a) $Gd_2O_3$ and (b) $GdTi_xO_y$ films annealed at various temperatures.
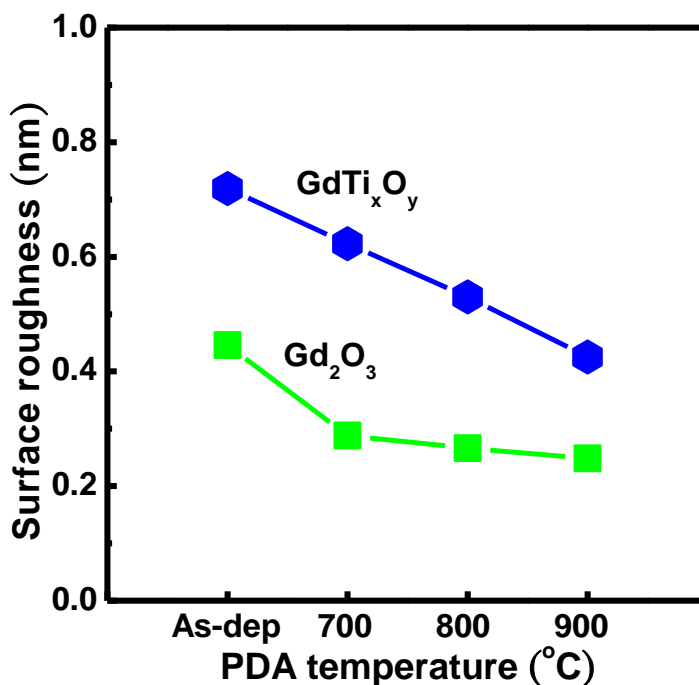


**Figure 2.** Surface roughness of $Gd_2O_3$ and $GdTi_xO_y$ films as a function of PDA temperatures.

The influence of thermal annealing at different PDA temperatures on the surface nature of $Gd_2O_3$ and $GdTi_xO_y$ sensing films, the outcome of AFM analysis was showed in Fig. 2. The as-deposited film exhibited a larger surface roughness than the annealed film. The enhancement in surface

roughness is possibly due to the moisture absorption of RE oxide films leading to the nonuniform volume expansion of the film [18]. The surface roughness of the $Gd_2O_3$ and $GdTi_xO_y$ films decreased with increasing the PDA temperature. We believe that these films are condensed during high temperature annealing as the density increase. In addition, the $GdTi_xO_y$ sample shows a higher surface roughness compared with the $Gd_2O_3$ sample. This is attributed to that the Ti adding into the $Gd_2O_3$ film increased the growth of the grain size.
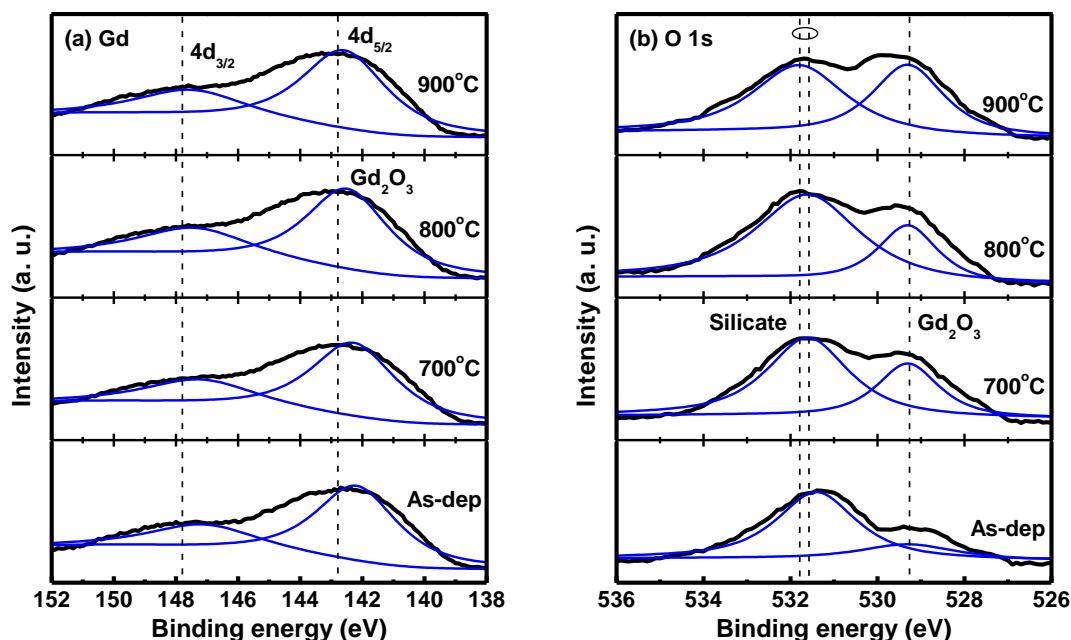


**Figure 3.** XPS spectra of (a) Gd 4d and (b) O 1s for $Gd_2O_3$ films annealed at various temperatures.

The effect of the annealing treatment on the compositional properties of the $Gd_2O_3$ and $GdTi_xO_y$ sensing films, XPS analysis was conducted. Figure 3(a) shows the Gd 4d XPS spectra for the $Gd_2O_3$ film after PDA treatment. The Gd $4d_{3/2}$ and $4d_{5/2}$ peaks of the reference $Gd_2O_3$ located at 147.9 and 142.8 eV [19], respectively. It is found that the Gd 4d double peaks of the as-deposited sample are shifted lower binding energy by about 0.5 eV as compared to the $Gd_2O_3$ reference position, suggesting a poor $Gd(OH)_x$ structure because of the hydroxide formation after exposure to an air ambient [20]. For the film annealed at 700 and 800 °C, The position of Gd 4d double peaks shifts to a higher binding energy relative to the $Gd(OH)_x$ position, suggesting a small amount of Gd reacting with OH causing a thinner $Gd(OH)_x$. The chemical shift of the Gd 4d doublet peaks moved toward higher binding energy for the film annealed 900 °C ($4d_{3/2}$ and $4d_{5/2}$ peaks at 147.7 eV and 142.6 eV, respectively) as compared to the sample annealed 700 and 800 °C. This shift is due to the high Gd-contented metal oxide film. The O 1s spectra for the $Gd_2O_3$ films after PDA at different temperatures are shown in Fig. 3(b) with their appropriate peak curve-fitting lines with respect to chemical states. Each fitting peak is assumed to follow the general shape of the Lorentzian-Gaussian function. In four sets of spectra, the O 1s peak at 529.3 eV represents the Gd-O bond [19], the O 1s peak at 531.4 eV assigns to the Gd-O-H bond, and the O 1s peak at 531.6 and 531.8 eV assigns to the Gd-O-Si bond [21]. It is evident that the

as-deposited film has only O 1s peak at 531.4 eV corresponding to Gd-(OH). This finding indicates that the reaction of $Gd_2O_3$ film with water causes the hydroxide formation in the $Gd_2O_3$ film. The O 1s peak intensity corresponding to $Gd_2O_3$ increased with increasing the PDA temperature. This finding is attributed to the reaction of oxygen with Gd atom forming a $Gd_2O_3$ structure. On the other hand, the shift of the O 1s peak (Gd silicate) for the sample annealed at 900 °C to a higher binding energy was increased by 0.2 eV. This is possibly due to the diffusion of oxygen atom from the high-k film to the $Gd_2O_3$/Si interface, resulting in the formation of a thicker Gd silicate layer.
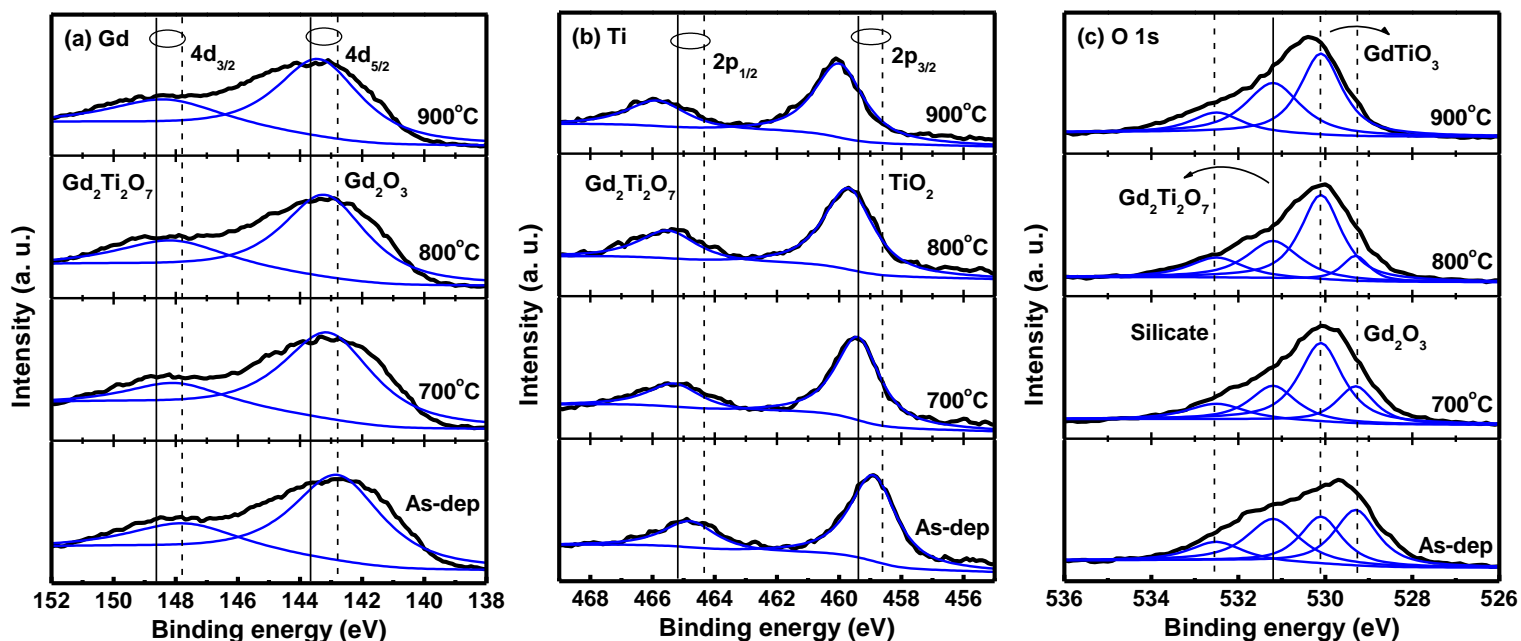


**Figure 4.** XPS spectra of (a) Gd 4d, (b) Ti 2p, and (c) O 1s for $GdTi_xO_y$ films annealed at various temperatures.

Figure 4 shows the Gd 4d, Ti 2p, and O 1s core level XPS spectra for the $GdTi_xO_y$ films annealed at different PDA temperatures. The binding energy of Gd $4d_{3/2}$ and $4d_{5/2}$ peaks at 148.7 and 143.7 eV can be assigned to the $Gd_2Ti_2O_7$ structure. The chemical shift to higher binding energy for Gd 4d double peaks indicates the difference between the Gd-O-Ti bonding in $Gd_2Ti_2O_7$ and that in $Gd_2O_3$. For the as-deposited sample, the Gd $4d_{3/2}$ and $4d_{5/2}$ peaks at 147.8 and 142.9 eV, respectively, suggest a poor crystal structure. It is found that the shift of the Gd 4d double peaks for annealed sample to a higher binding energy increases with increasing the PDA temperature. This can be explained by the formation of a better crystal structure during high temperature annealing. For the film annealing at 900 °C, the chemical shift of the Gd 4d double peaks moved toward high binding energy for the case of the $GdTi_xO_y$ film ($4d_{3/2}$ and $4d_{5/2}$ peaks at 148.5 and 143.5 eV, respectively). It should be noted that the peak of the Ti $2p_{1/2}$ and $2p_{3/2}$ energy levels appeared at 464.9 and 458.9 eV for the as-deposited film [Fig. 4(b)], respectively, indicating a poor crystal structure incorporating Ti in the form of TiOH, which probably formed in the surface region of the sample during its exposure to air [12]. For the film annealed at 900 °C, the Ti 2p doublet (Ti $2p_{1/2}$ and Ti $2p_{3/2}$ at 465.9 and 460 eV,

respectively) is shifted to higher binding energy compared to the $Gd_2Ti_2O_7$ reference position (Ti $2p_{1/2}$ and Ti $2p_{3/2}$ at 465.2 and 459.4 eV, respectively) [22]. This shift was attributed to Ti in $GdTi_xO_y$ compound consisting of $Gd_2Ti_2O_7$ and $GdTiO_3$. Figure 4(c) displays the O 1s spectra with appropriate curve-fitting of peaks for the $GdTi_xO_y$ films after PDA treatment. In the four sets of spectra, the O 1s peaks at 529.3, 530.1, 531.2, and 532.5 eV represent the Gd–O ($Gd_2O_3$), Gd–O–Ti ($GdTiO_3$), Gd–O–Ti ($Gd_2Ti_2O_7$), and Gd–O–Si ($GdSi_xO_y$) bonds [21-22], respectively. The as-deposited film exhibited one weak Gd silicate and three strong $Gd_2Ti_2O_7$ $GdTiO_3$, and $Gd_2O_3$ peaks, suggesting a poorly crystalline structure. The O 1s peak intensity corresponding to $Gd_2O_3$ decreased with increasing the PDA temperature, whereas the O 1s peak intensity with respect to $Gd_2Ti_2O_7$ increased accordingly. This phenomenon is consistent with the reaction of O and Gd atoms with Ti atoms, forming a well-crystallized $Gd_2Ti_2O_7$ film. Furthermore, the O 1s peak intensity corresponding to $GdTiO_3$ remained rather constant for annealed sample. This result is in good agreement with the XRD data showing several intensive diffraction peaks. The O 1s peak corresponding to the Gd silicate components of the film annealed at 800 °C had higher intensity compared to 700 °C, suggesting that Gd atoms diffused from the oxide film to form a thicker Gd silicate layer at the oxide–Si interface.

### 3.2. Sensing characterization

The reference voltage ($V_{REF}$) related to the surface potential ($\psi$) depends on the acido-basic properties of the sensing film and the electrolyte pH. The value of $\psi$ can be determined from the equation 1

$$\psi = 2.303 \frac{kT}{q} \frac{\beta}{\beta+1} (pH_{pzc} - pH) \dots\dots\dots\dots\dots\dots\dots\dots\dots\dots eq.\ 1$$

where $k$ is Boltzmann's constant, $T$ is the temperature of the system, $q$ is the elementary charge, $pH_{pzc}$ is the pH at the point of zero charge, and $\beta$ is a parameter that indicates the chemical sensitivity of the gate oxide. The $pH_{pzc}$ of pH-ISFET is given by the equation 2

$$pH_{pzc} = -\log_{10}\left(\frac{K_a}{K_b}\right)^{0.5} \dots\dots\dots\dots\dots\dots\dots\dots\dots\dots\dots\dots\dots eq.\ 2$$

where $K_a$ and $K_b$ denote the equilibrium constants at acid and base point, respectively. In addition, the $\beta$ value is related to the chemical sensitivity of gate oxide and is determined by the density of surface hydroxyl groups, which is given as the equation 3.

$$\beta = \frac{2q^2 N_s \sqrt{K_a K_b}}{kTC_{DL}} \dots\dots\dots\dots\dots\dots\dots\dots\dots\dots\dots\dots\dots eq.\ 3$$

where $N_s$ is the total number of surface site per unit area and $C_{DL}$ is the double layer capacitance derived from the Gouy-Chapman-Stern model [23]. In pH-EIS sensing, the change in the pH of the solution caused a shift in the reference voltage of the *C–V* curves.
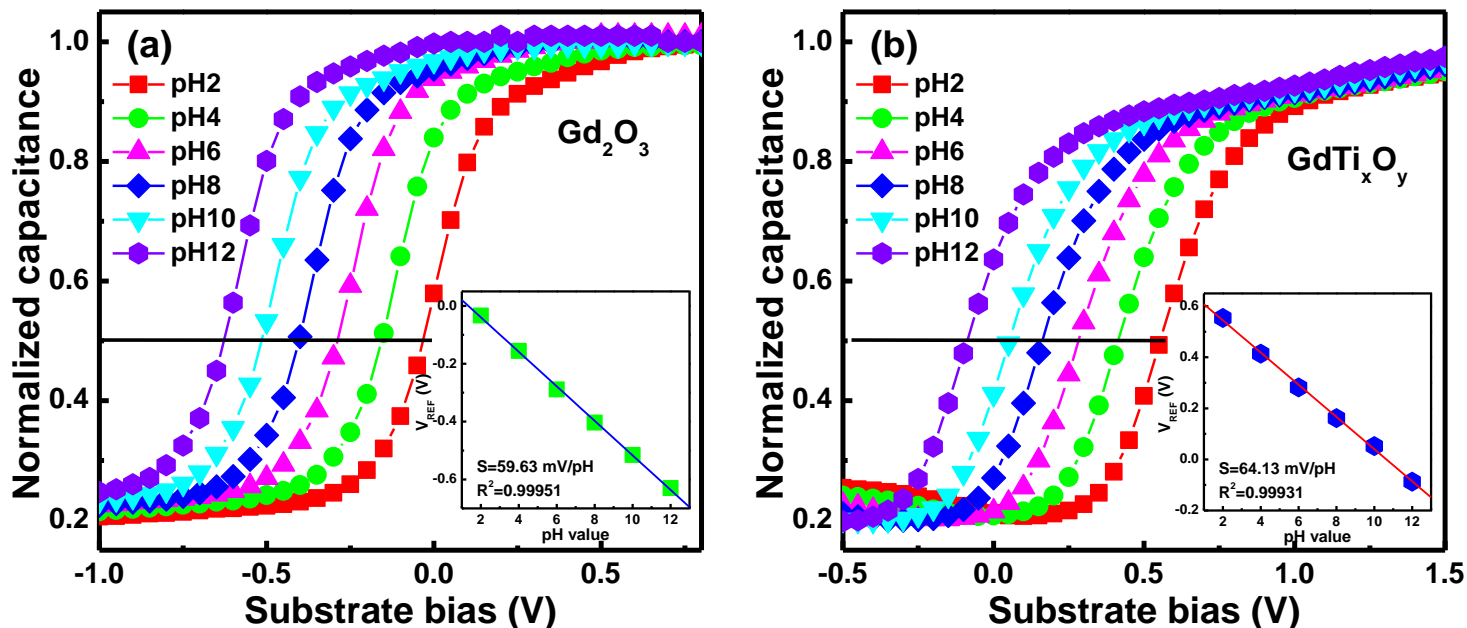


**Figure 5.** C-V curves response of (a) $Gd_2O_3$ and (b) $GdTi_xO_y$ EIS devices with annealing at 900 °C when inserted into solutions with pH values from 2 to 12. The inset shows the reference voltage of (a) $Gd_2O_3$ and (b) $GdTi_xO_y$ EIS devices with annealing at 900 °C as a function of pH values.

This result is mainly due to the ionization of the surface hydroxyl groups by either hydrogen ions or hydroxyl ions. The effect of the PDA temperature on the pH sensitivity of the $Gd_2O_3$ and $GdTi_xO_y$ sensing films can be realized by using the site-binding model to describe the ionic absorption processes at the electrolyte/oxide interface [24].

Figures 5(a) and (b) demonstrate the pH dependence of one group of *C–V* curves for the $Gd_2O_3$ and $GdTi_xO_y$ EIS devices annealed at 900 °C. These normalized *C–V* curves were shifted as a result of $H^+$ ions modifying the surface potential through dipole formation on the sensing membrane. This EIS device has distorted *C–V* curves in the solutions from pH 2 to 12. This may be attributed to the presence of interface traps in the oxide. A set of C-V curves was measured as a function of different pH solutions to determine the pH sensitivity of the sensing film. The inset of Fig. 5(a) and (b) displays the reference voltage (the voltage required to achieve a normalized capacitance of 0.5) of $Gd_2O_3$ and $GdTi_xO_y$ sensing membranes after PDA at 900 °C as a function of pH, respectively. During a cycle from pH 2 to 12, such a $GdTi_xO_y$ EIS device exhibits a higher pH sensitivity of 64.13 mV/pH compared with $Gd_2O_3$ EIS device.

To evaluate the sensing performance of the $Gd_2O_3$ and $GdTi_xO_y$ EIS devices after PDA at different temperatures, we recorded a set of *C–V* curves at the pH ranging from pH 2 to 12. The pH

sensitivity of $Gd_2O_3$ and $GdTi_xO_y$ EIS devices as a function of PDA temperatures is shown in Fig. 6. The pH sensitivity of EIS device increases with increasing the PDA temperature. In addition, $GdTi_xO_y$ EIS device exhibits a higher pH sensitivity than $Gd_2O_3$ EIS one.
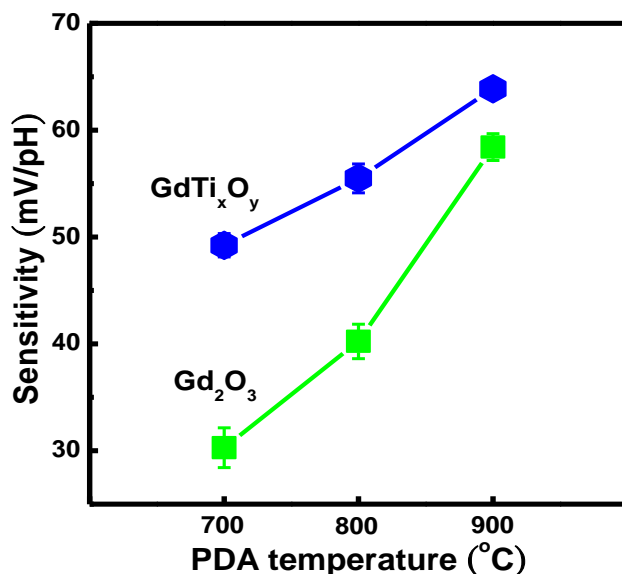


**Figure 6.** pH sensitivity as a function of PDA temperatures for high-$\kappa$ $Gd_2O_3$ and $GdTi_xO_y$ EIS devices.
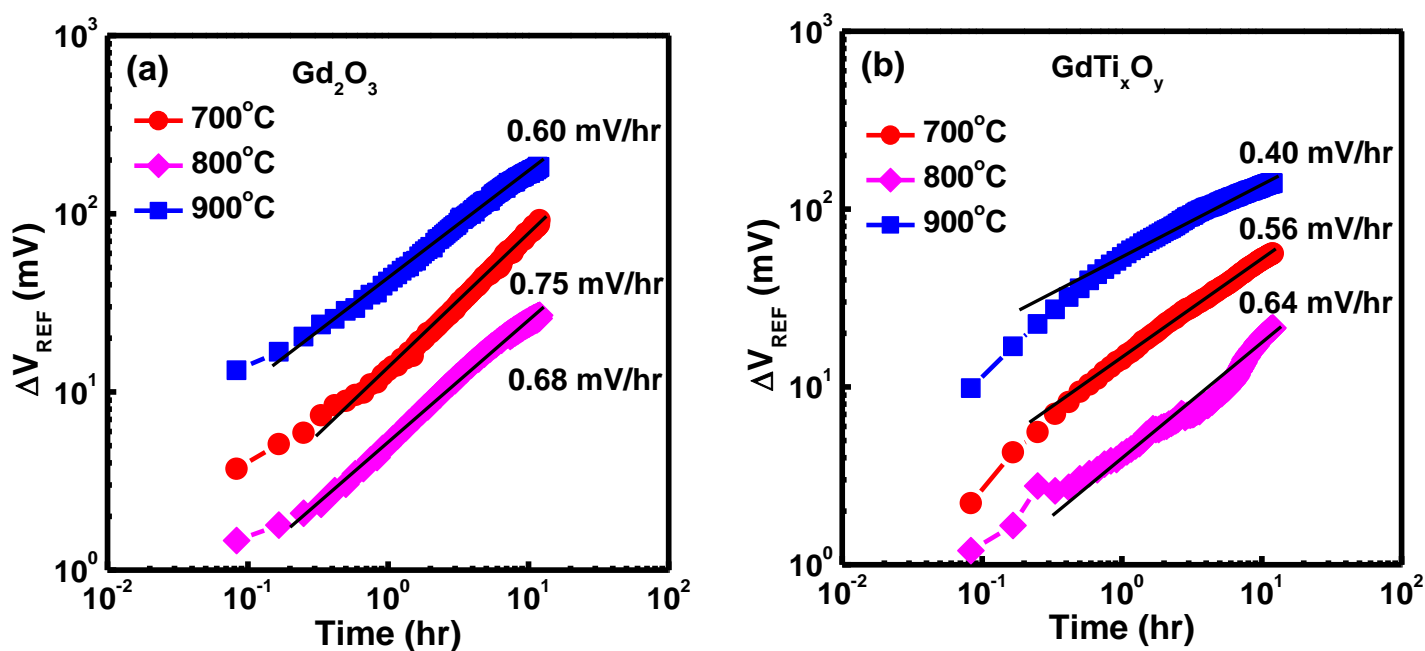


**Figure 7.** Drift characteristics as a function of times for (a) $Gd_2O_3$ and (b) $GdTi_xO_y$ EIS devices annealed at various temperatures, measured in the pH= 7 solution.
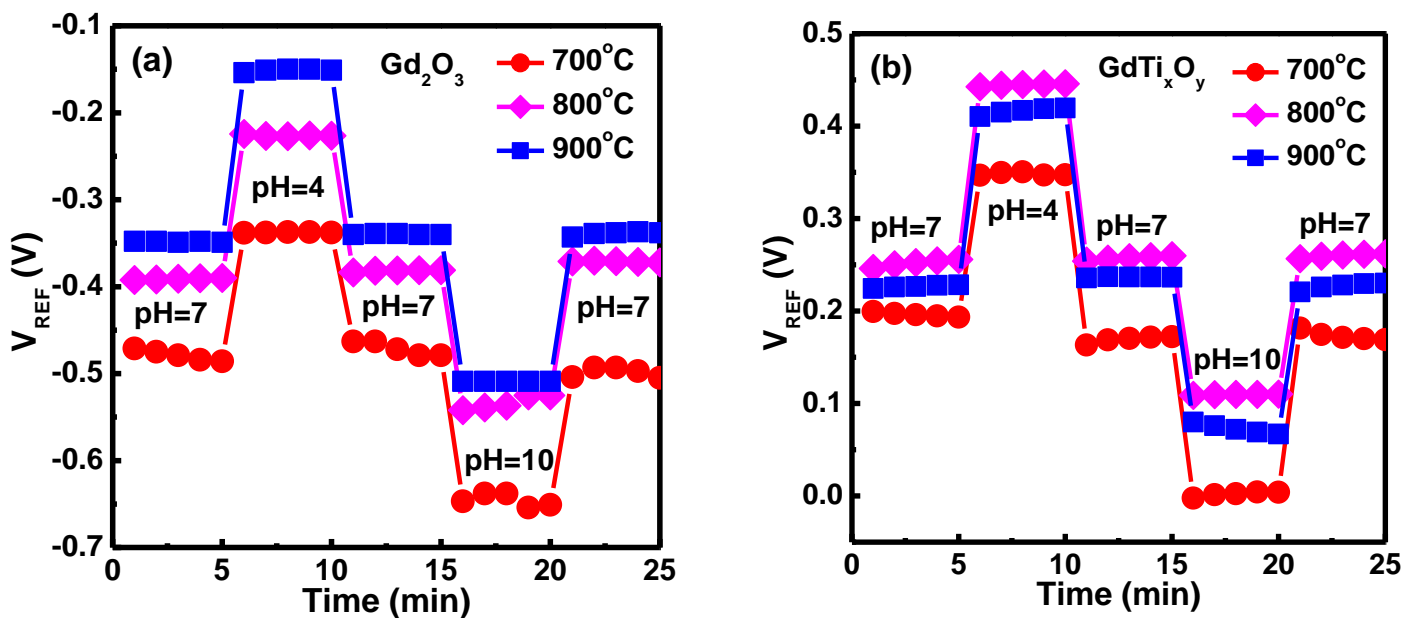
**Figure 8.** Hysteresis characteristics of (a) $Gd_2O_3$ and (b) $GdTi_xO_y$ EIS devices annealed at different temperatures during the pH loop of 7→4→7→10→7.
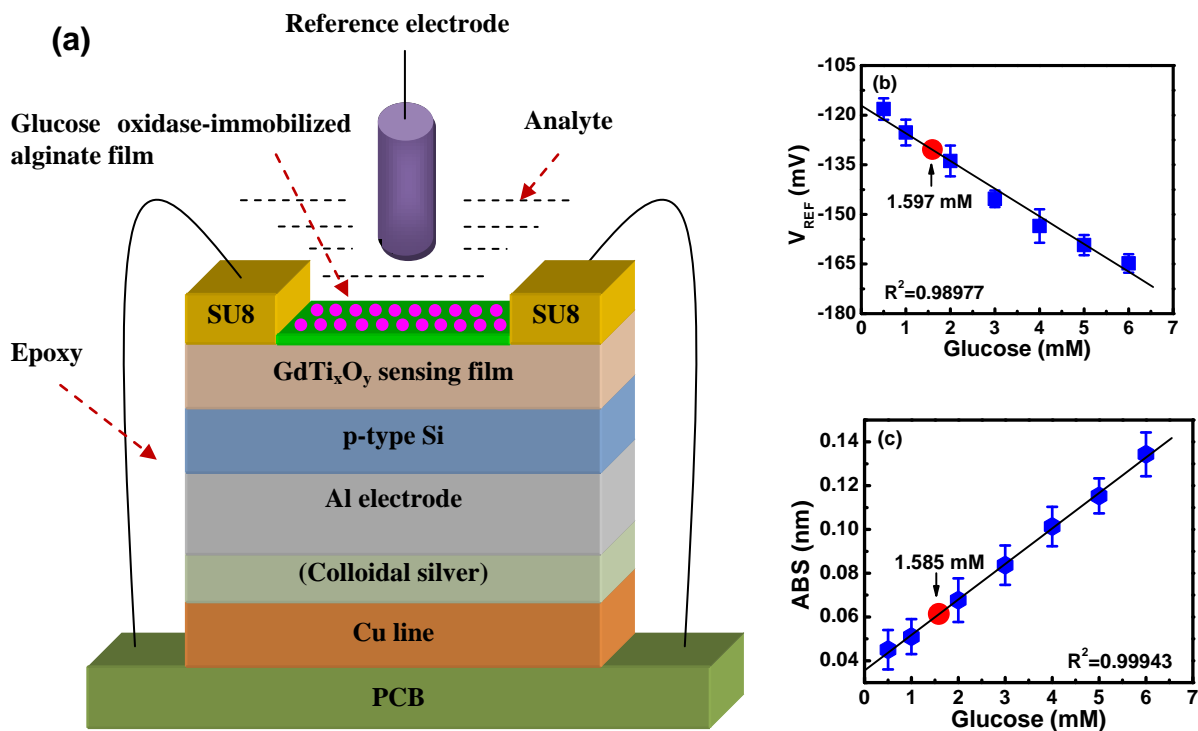


**Figure 9.** (a) Scheme of hybrid configuration of a glucose EIS biosensor. The typical calibration curves of (b) $GdTi_xO_y$ EIS glucose biosensor and (c) glucose assay kit.

This result could be attributed to the higher surface roughness of the $GdTi_xO_y$ sensing film as observed in the previous AFM analysis. With the higher surface roughness, the number of surface sites will increase accordingly, which, therefore, contributes to a higher detection sensitivity as previously our discussed in the site-binding model [25]. We find that the $GdTi_xO_y$ sensing membrane annealed at 900 °C has a higher pH sensitivity of 64.13 mV/pH than other PDA temperatures. This result is attributed to the $Gd_2Ti_2O_7$ and $GdTiO_3$ combining a $GdTi_xO_y$ compound.

Figures 7(a) and (b) show the drift characteristics of $Gd_2O_3$ and $GdTi_xO_y$ EIS devices annealed at various temperatures as a function of time, measured in the pH 7 solutions for 12 h. The drift rate of a pH-ISFET can be explained through the penetration of ions contained in the electrolyte into the sensing membrane [26]. The charged electrolyte ions can penetrate the hydrated layer of the sensing membrane and cause the decrease in effective gate oxide thickness [27]. Therefore, the change of gate capacitance induces the non-ideal effects in the ISFETs. The total amount of penetrating ions and the duration of the penetration process depend on the ion mobility of the sensing membrane. The change in the reference voltage can be written as $\Delta V_{REF}=V_{REF}(t)-V_{REF}(0)$. The degradation slope of the reference voltage variation reflects the stability of an EIS device. The $GdTi_xO_y$ EIS device annealed at 900 °C exhibited the best long-term stability (slope=0.4 mV/h); in contrast, the $Gd_2O_3$ EIS capacitor featured a high drift of 0.6 mV/h. The small drift effect resulted from the low mobility of ions due to the low density of crystal defects in the film, while a high drift rate is attributed to a larger number of crystal defects producing the high mobility of ions.

**Table 1.** Comparison of sensing parameters for an EIS device fabricated with a $Si_3N_4$, $Ta_2O_5$, $Al_2O_3$, $HfO_2$, $Sm_2O_3$, $Dy_2TiO_5$, $Gd_2O_3$, and $GdTi_xO_y$.

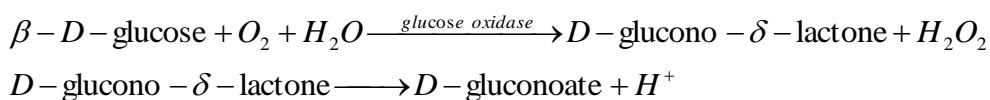| Sensing membrane | pH sensivity (mV/pH) | Hysteresis voltage (mV) | Drift rate (mV/h) |
|:---:|:---:|:---:|:---:|
| $Si_3N_4$ | 53-55 | 3 | 0.8 |
| $Ta_2O_5$ | 55-58 | < 1 | 0.2 |
| $Al_2O_3$ | 54-56 | 0.8 | 0.3 |
| $HfO_2$ | 58.3 | 1.7 | 0.6 |
| $Sm_2O_3$ | 56.2 | 6.2 | 1.29 |
| $Dy_2TiO_5$ | 57.59 | 0.2 | 0.362 |
| $Gd_2O_3$ | 59.63 | 9.4 | 0.6 |
| $GdTi_xO_y$ | 64.13 | < 1 | 0.4 |

Figures 8(a) and (b) depict the hysteresis phenomenon of $Gd_2O_3$ and $GdTi_xO_y$ EIS devices annealed at different temperatures, measured under the pH loop of 7→4→7→10→7 over a period of 1500 s. Hysteresis phenomenon can be explained by the defects of an insulator film, resulting in the formation of porous structures [28]. The interior sites of these porous defects could react with the ions existing in the tested solution and thus causes hysteresis response. The hysteresis voltage here is

defined as the reference voltage difference between the initial and terminal voltages measured in the above cycle. The EIS device incorporating a $GdTi_xO_y$ sensing film exhibits a smaller hysteresis voltage than that of $Gd_2O_3$ film. This outcome is attributed to the fast response of such a $GdTi_xO_y$ EIS device due to a better $GdTi_xO_y$ structure and a lower defect chemistry. Furthermore, the $GdTi_xO_y$ EIS device annealed at 900 °C had a lower hysteresis voltage of ~1 mV than other annealing temperatures. This may be attributed to a low number of crystal defects. In contrast, the 700 °C-annealed sample shows a high hysteresis voltage variation (23 mV), suggesting a large density of crystal defects to create interior sites. These would be sites that can respond to changes of the chemical composition of the tested solution, leading to large variations in the reference voltage.

The measured as well as extracted sensing parameters are summarized in Table 1, where the data from EIS devices incorporating a $Si_3N_4$ [29-30], $Ta_2O_5$ [31], $Al_2O_3$ [29-30], $HfO_2$ [32], $Sm_2O_3$ [33], and $Dy_2TiO_5$ [34], are shown for comparison. Our present $GdTi_xO_y$ sensing film exhibits superior better pH sensitivity. Although the $GdTi_xO_y$ EIS device did feature slightly high values of hysteresis and drift, the thickness of the $GdTi_xO_y$ sensing film can be decreased to lower these values.

### 3.3. $GdTi_xO_y$ EIS glucose biosensor

In this study, we demonstrated a $GdTi_xO_y$ EIS biosensor with glucose oxidase-immobilized alginate film to detect directly glucose in serum. Fig. 9(a) illustrates the hybrid configuration of a $GdTi_xO_y$ EIS biosensor. Since the measurement was carried out in serum, a layer of alginate gel could serve as a filter membrane to possibly avoid the contact of biomolecules with oxide surface, which may prevent unnecessary interference during the detection. Glucose oxidase is a well-known enzyme that catalyzes the oxidation of glucose to yield gluconic acid and hydrogen peroxide while consuming oxygen [35], as described in the reaction.

$$\beta - D - \text{glucose} + O_2 + H_2O \xrightarrow{\quad glucose\ oxidase \quad} D - \text{glucono} - \delta - \text{lactone} + H_2O_2$$
$$D - \text{glucono} - \delta - \text{lactone} \longrightarrow D - \text{gluconate} + H^+$$

In the enzymatic reaction of glucose, the amount of gluconic acid is proportional to the concentration of the glucose and the subsequent dissociation of glucose acid generates the hydrogen ions. As a result, the underlying EIS sensor can detect an increase of local pH in the biomembrane upon addition of glucose. Fig. 9(b) demonstrates that the $V_{REF}$ value shows a linear dependence on the concentration of glucose in the range from 0.5 mM to 6 mM. It is found that the slope of calibration curve of glucose is negative, suggesting that the increase in glucose concentration causes local pH increase near the oxide layer and thus decreases the $V_{REF}$ value of EIS biosensor. Based on the calibration curve, the sensitivity of a $GdTi_xO_y$ EIS sensor for glucose is about 8.37 mV/mM. It is noteworthy that ISFET devices are often influenced by the change in ionic strength of the solution [36]. In order to avoid the inference from considerable salt content in serum, the serum sample was

diluted by 1X PBS to ensure that the change in the $V_{REF}$ was only induced by the local pH change in the biomembrane. Furthermore, the dilution treatment allows the buffer capacity of serum is similar to those of standard solutions of glucose [37]. As shown in Fig 9(b), a red circle represents the averaged reference voltages (130.4 mV) from 3 times measurements of serum sample, which also correspond to the serum glucose at a concentration of 1.597 mM. In order to verify the accuracy of a $GdTi_xO_y$ EIS biosensor, glucose assay kit was used to quantify its concentration in diluted serum and the measured value was directly compared with the one estimated by a $GdTi_xO_y$ EIS biosensor. As shown in Fig 9(c), the standard curve of glucose assay kit displays a good linearity ($R^2 = 0.99$) and thus the concentration of glucose in diluted serum can be calculated as 1.585 mM [red circle in Fig. 9(c)]. This concentration level is nearly identical to the value determined by a $GdTi_xO_y$ EIS biosensor with glucose oxidase immobilized alginate film, suggesting our device is able to accurately quantify the concentration of glucose in serum. Because we demonstrated that a $GdTi_xO_y$ EIS biosensor exhibited high sensitivity to pH change and the ability of quantifying the biomolecules under a physiological condition, it is expected that this biosensor can potentially serve as the diagnosis tool for general clinical examinations.

## 4. CONCLUSION

We have developed a highly pH sensitive EIS sensor with a thin layer of $Gd_2O_3$ and $GdTi_xO_y$ by using sputtering technique. We employed XRD, XPS, and AFM analyses to confirm the presence of $Gd_2O_3$ and $GdTi_xO_y$ structures in the EIS devices. The $GdTi_xO_y$ EIS device with annealing at 900 °C exhibited a higher sensitivity (64.13 mV/pH), a smaller hysteresis voltage (1 mV), and a lower drift rate (0.4 mV/h), relative to those of the systems that had been subjected to other annealing conditions. This result is attributed to the combination of $Gd_2Ti_2O_7$ and $GdTiO_3$ forming a $GdTi_xO_y$ compound and its higher surface roughness. Finally, we successfully demonstrate the use of $GdTi_xO_y$ EIS with glucose oxidase-immobilized alginate film for the detection of serum glucose. The $GdTi_xO_y$ EIS glucose biosensor shows a good linearity ($R^2 = 0.99$) in the concentration range of 0.5-6 mM. Furthermore, the sensitivity of glucose oxidase immobilized EIS biosensor for glucose is about 8.37 mV/mM. The concentration of serum glucose measured by a $GdTi_xO_y$ EIS biosensor is nearly identical to that determined by commercial assay kit. It is expected that a highly sensitive $GdTi_xO_y$ EIS based biosensor is promising for the extended application on general clinical diagnosis.

## References

1.  P. Bergveld, *IEEE Trans. Biomed. Eng.*, 17 (1970) 70.

2.  S. V. Dzyadevych, A. P. Soldatkin, A. V. Elskaya, C. Martelet, and N. Jaffrezic-Renault, *Anal. Chim. Acta*, 568 (2006) 248.
3.  M. J. Schoning and A. Poghossian, *Electroanalysis*, 18 (2006) 1893.
4.  T. M. Pan, C. D. Lee and M. H. Wu, *J. Phys. Chem. C*, 113 (2009) 21937.
5.  J. L. Her, C. W. Lin, K. Y. Chang, and T. M. Pan, *Int. J. Electrochem. Sci.*, 7 (2012) 387.
6.  G. D. Wilk, R. M. Wallace, and J. M. Anthony, *J. Appl. Phys.*, 89 (2001) 5243.
7.  M. Houssa, *High-k Gate Dielectrics*, Institute of Physics, London (2004).
8.  M. Fanciulli and G. Scarel (Eds.), *Rare Earth Oxide Thin Film: Growth, Characterization, and Applications*, Springer, Berlin (2007).
9.  J. Paivasaari, M. Putkonen, and L. Niinisto, *Thin Solid Films*, 472 (2005) 275.
10. O. Engstrom, B. Raeissi, S. Hall, O. Buiu, M. C. Lemme, H. D. B. Gottlob, P. K. Hurley, and K. Cherkaoui, *Solid State Electron.*, 51 (2007) 622.
11. H. Ono and T. Katsumata, *Appl. Phys. Lett.*, 78 (2001) 1832.
12. S. Jeon and H. Hwang, *J. Appl. Phys.*, 93 (2003) 6393.
13. M. H. Cho, D. W. Moon, S. A. Park, Y. S. Rho, Y. K. Kim, K. Jeong, C. H. Chang, J. H. Gu, J. H. Lee, and S. Y. Choi, *Appl. Phys. Lett.*, 84 (2004) 678.
14. A. Laha, E. Bugiel, H. J. Osten and A. Fissel, *Appl. Phys. Lett.*, 88 (2006) 172107.
15. R. B. van Dover, *Appl. Phys. Lett.*, 74 (1999) 3041.
16. S. Jeon and H. Hwang, *Appl. Phys. Lett.*, 81 (2002) 4856.
17. T. M. Pan and C. H. Lu, *Thin Solid Films*, 519 (2011) 8149.
18. Y. Zhao, M. Toyama, K. Kita, K. Kyuno, and A. Toriumi, *Appl. Phys. Lett.*, 88 (2006) 072904.
19. Y. A. Teterin and A. Y. Teterin, *Russ. Chem. Rev.*, 71 (2002) 347.
20. Y. Zhao, K. Kita, K. Kyuno, and A. Toriumi, *Appl. Phys. Lett.*, 89 (2006) 252905.
21. J. F. Moulder, W. F. Stickle, P. E. Sobol, and K. D. Bomben, *Handbook of X-Ray Photoelectron Spectroscopy: A Reference Book of Standard Spectra for Identification and Interpretation of XPS Data*, Physical Electronics, Eden Prairie, MN (1995).
22. J. Chen, J. Lian, L. M. Wang, R. C. Ewing, and L. A. Boatner, *Appl. Phys. Lett.*, 79 (2001) 1989.
23. R. E. G. van Hal, J. C. T. Eijkel, and P. Bergveld, *Sens. Actuators B*, 24 (1995) 201.
24. C. D. Fung, P. W. Cheung, and W. H. Ko, *IEEE Trans. Electron Devices*, 33 (1986) 8.
25. T. M. Pan, K. Y. Chang, C. W. Lin, S. W. Tsai, and M. H. Wu, *Sen. Actuators B*, 160 (2011) 850.
26. C. C. Wen, T. C. Chen, and J. N. Zemel, *IEEE Trans. Electron Devices*, 26 (1979) 1945.
27. L. Bousse, S. Mostarshed, B. van der Schoot, and N. F. de Rooij, *Sens. Actuators B*, 17 (1994)157.
28. L. Bousse, H. H. van den Vlekkert, and N. F. de Rooij, *Sens. Actuators B*, 2 (1990) 103.
29. Y. Miao, J. Guan, and J. Chen, *Biotechnol. Adv.*, 21 (2003) 527.
30. T. Matsuo, M. Esashi, and H. Abe, *IEEE Trans. Electron Devices*, 26 (1979).
31. A. Poghossian and M. J. Schoning, *Electroanalysis*, 16 (2004) 1863.
32. C. M. Yang, C. S. Lai, T. F. Lu, T. C. Wang, and D. G. Pijanowska, *J. Electrochem. Soc.*, 155 (2008) J326.
33. M. H. Wu, C. H. Cheng, C. S. Lai, and T. M. Pan, *Sen. Actuators B*, 138 (2009) 221.
34. T. M. Pan and C. W. Lin, *J. Phys. Chem. C*, 114 (2010) 17914.
35. B. R. Eggins, *Chemical Sensors and Biosensors*, John Wiley & Sons, New York (2002).
36. A. P. Soldatkin, A. V. Elskaya, A. A. Shulga, L. I. Netchiporouk, A. M. Nyamsi Hendji, N. Jaffrezic-Renault, and C. Martelet, *Anal. Chim. Acta*, 283 (1993) 695.
37. X. L. Luo, J. J. Xu, W. Zhao, and H. Y. Chen, *Biosens. Bioelectron.*, 19 (2004) 1295.